Vietnam Journal of Science and Technology ***64***(1) (2026) 78–86
DOI: https://doi.org/10.15625/2525-2518/18821

Synthesis and properties of g-C_3N_4 bulk and nanosheet from thiourea

Luu Thi Lan Anh[1], Nguyen Quang Truong[1], Nguyen Thi Tuyet Mai[2], Nguyen Cong Tu[1], Le Manh Cuong[3,*]

[1]*Faculty of Engineering Physics, Hanoi University of Science and Technology, 1 Dai Co Viet, Hai Ba Trung, Ha Noi, Viet Nam*
[2]*School of Chemistry and Life Sciences, Hanoi University of Science and Technology, 1 Dai Co Viet, Hai Ba Trung, Ha Noi, Viet Nam*
[3]*Faculty of Building Materials, Hanoi University of Civil Engineering, 55 Giai Phong, Hai Ba Trung, Ha Noi, Viet Nam*

[*]Email: *cuonglm@huce.edu.vn*

Received: 5 September 2023; Accepted for publication: 5 June 2025

Abstract. Graphitic carbon nitride (g-C_3N_4) is a metal-free polymer semiconductor of interest for visible-light photocatalysis. Here, the g-C_3N_4 bulk was prepared by thermal polycondensation of thiourea in air (480–550 °C, 2 h; 5 °C min^{-1}). XRD and FTIR analysis confirmed the heptazine/triazine framework, with well-defined (002) and (100) reflections obtained at 520–550 °C, while lower temperatures showed incomplete condensation. Few-layer g-C_3N_4 nanosheets were then produced by thermal oxidation/exfoliation of the bulk at 500 °C in static air, yielding an expanded, porous morphology observed by FESEM and a weaker (002) peak together with an additional feature near 23°. Optical characterization (UV–Vis DRS and PL) indicated improved light utilization and charge-carrier behavior for the nanosheets: the optical bandgap decreased from 2.750 eV (bulk) to 2.625 eV (nanosheets) and the PL maximum blue-shifted (≈465 → 444 nm) with lower intensity, suggesting suppressed electron–hole recombination. Lorentz deconvolution of PL spectra revealed three main emission centers associated with distinct transition pathways. This simple, solvent-free route using low-cost thiourea provides scalable g-C_3N_4 bulk and nanosheets for visible-light-driven environmental and energy applications.

Keywords: graphitic carbon nitride, g-C_3N_4 nanosheet, thiourea precursor, polymerization, photocatalytic materials.

Classification numbers: 2.4.2, 2.1.3.

1. INTRODUCTION

Graphitic carbon nitride (g-C_3N_4) is the most stable allotrope of carbon nitride (C_3N_4) at room temperature [1]. Owing to its high thermal and chemical stability, low-cost and abundant elements, environmental friendliness, and suitable band structure aligned with water redox potentials, g-C_3N_4 has been widely studied for photocatalytic applications [2, 3]. It exhibits activity in organic pollutant degradation [4], water splitting for H_2 and O_2 production [5], and CO_2 reduction to hydrocarbon fuels [6]. However, its photocatalytic performance is limited by

the high recombination rate of photogenerated electron–hole pairs and a low density of active sites [7].

Two-dimensional (2D) g-C_3N_4 nanosheets exhibit a large specific surface area, which enhances reactive sites, accelerates mass transfer, and improves light absorption. Compared with bulk g-C_3N_4, 2D nanosheets also promote charge separation and prolong carrier lifetime [8–14]. Various synthesis strategies have been reported, including in situ polymerization methods [15], thermal exfoliation [16,17], chemical exfoliation [18], and plasma-assisted techniques [19].

In this work, the bulk g-C_3N_4 was synthesized via single-step thermal polycondensation of thiourea. The influence of thiourea precursors on structural formation and properties was investigated. Furthermore, nanosheets were obtained by thermal exfoliation of the bulk material in air to evaluate the structural and optical modifications induced by exfoliation.

2. MATERIALS AND METHODS

2.1. Materials

Thiourea was purchased from Sigma-Aldrich with analytical grade purity and used without further purification.

2.2. Synthesis of g-C_3N_4bulk and nanosheets

The g-C_3N_4 bulk was synthesized by a thermal polymerization method using thiourea precursors. In a typical synthesis, 10 g of thiourea were placed in a porcelain crucible with a cover and heated at temperatures of 480, 500, 520, and 550 °C in air at a rate of 5 °C/min for 2 hours. After cooling to room temperature, the resulting pale-yellow product was collected.

Nanosheets were prepared by thermal exfoliation of the obtained g-C_3N_4bulk. Specifically, 0.5 g of the bulk sample were placed in an open porcelain crucible and heated at 500 °C in air for 2 hours at a rate of 5 °C/min. The resulting light-yellow powder was collected as g-C_3N_4 nanosheets. Figure 1 presents the diagram of the synthesisof g-C_3N_4 bulk and nanosheet.

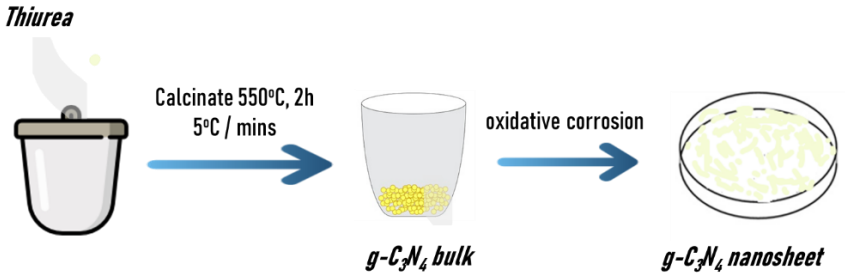

Figure 1. Diagram of synthesisof g-C_3N_4 bulk and nanosheet.

2.3. Characterization

The crystal structure and phase purity were obtained using X'pert Pro (PANalytical) MPD with CuK-α1 radiation (= 1.54056 Å) at a scanning rate of 0.03°/2s in the 2θ range from 10° to 70°. The crystal analysis was performed by HighScore Plus software using the ICDD database. FTIR spectra were analyzed using FT/IR-4600 type A (JASCO) with a wavenumber range from

500 cm^{-1} to 4000 cm^{-1}. The morphology of the samples was investigated using a HITACHI S4800 field emission scanning electron microscope (FESEM, Japan). The diffusion reflectance of the samples was measured on a JASCO V-750 instrument using a 60 mm ISV-922 integrating sphere with a scanning rate of 200 nm/min and a UV-vis bandwidth of 0.50 nm. The photoluminescence (PL) properties of the g-C_3N_4 samples were measured.

3. RESULTS AND DISCUSSION

3.1. Structural characterization of the material

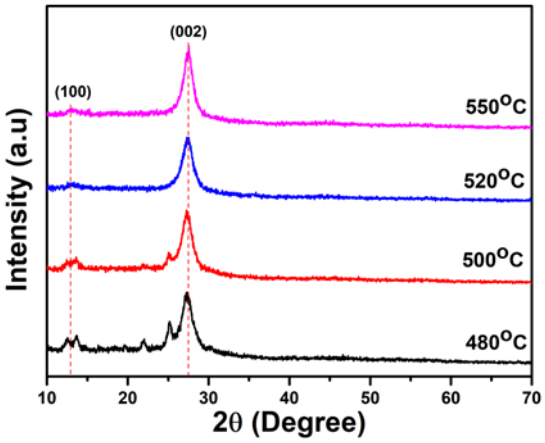

Figure 2. XRD patterns of g-C_3N_4 polymerization at different temperatures.

Figure 2 shows the XRD patterns of g-C_3N_4 synthesized by polymerization method from thiourea. The results showed that all samples synthesized exhibited the appearance of two diffraction peaks, in which a strong diffraction peak at angle 2θ = 27.40° corresponds to the diffraction planes (002), characterizing the superposition of aromatic conjugate systems; Another weaker diffraction peak at 2θ = 12.78° corresponds to the diffraction surface (100), which characterizes the cyclic arrangement of tri-s-triazine or heptazine structural units. Furthermore, the samples synthesized at 500 °C and 480 °C showed the presence of other diffraction peaks indicating incomplete formation of g-C_3N_4 for thiourea. The samples at 520 °C and 550 °C show that the diffraction peaks of g-C_3N_4 are consistent with the standard tag JCPDS number 87-1526 of g-C_3N_4 and previously published results [1, 20].

To investigate the vibrations of organic functional groups, the samples were analyzed using the FTIR method. FTIR spectra of g-C_3N_4 polymerization at different temperatures are presented in Figure 3 in the range of 500 - 4000 cm^{-1}. Typical absorption bands related to the vibration characteristic of g-C_3N_4 appeared in all samples. The NH stretching vibration mode from the surface uncondensed amine groups is assigned to the broadband between 3500 cm^{-1} and 3000 cm^{-1}. Bands between 1700 ~1000 cm^{-1} are assigned to the C=N extension bonds. Prolonged valence oscillations of C-N bonds in aromatic conjugate rings at 1569 cm^{-1} to 1247 cm^{-1}. The two peaks located between 806 and 884 cm^{-1} are derived from the binding of triazine units, indicating that the molecular structure of the prepared g-C_3N_4 consists of triazine units [21]. The results agreed well with the XRD results.

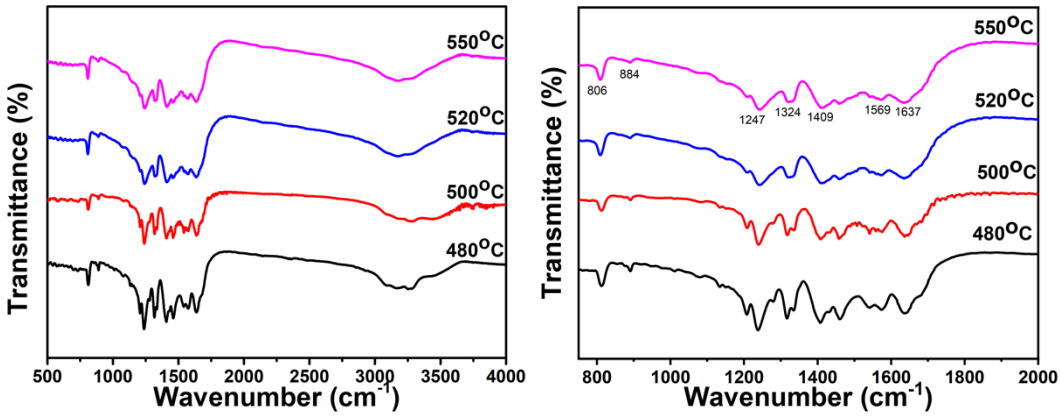

Figure 3. FTIR spectra of g-C_3N_4 calcination at different temperatures.

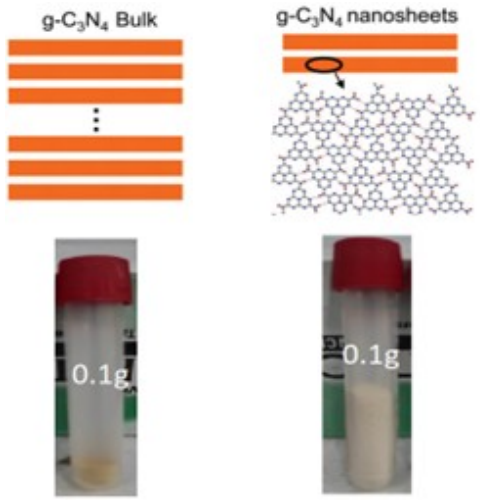

Figure 4. Images of g-C_3N_4 bulk and nanosheet.

The images of the g-C_3N_4 bulk and nanosheet are given in Figure 4. The volume of the nanosheets with the same weight is much larger than that of the bulk g-C_3N_4, indicating the fluffy state of the nanosheets.

3.2. Morphological characterization of the material

The morphology of g-C_3N_4 bulk and nanosheets were investigated with FESEM as shown in Figure 5. Compared to their parent bulk material consisting of solid agglomerates with a size of several micrometers (Figure 5(a)), the representative nanosheets appear as loose and soft agglomerates with a size of tens of micrometers (Figure 5(b)). This can be easily understood due to the gradual oxidation decomposition of the strands of polymeric melon units in the layers of bulk g-C_3N_4 during etching.

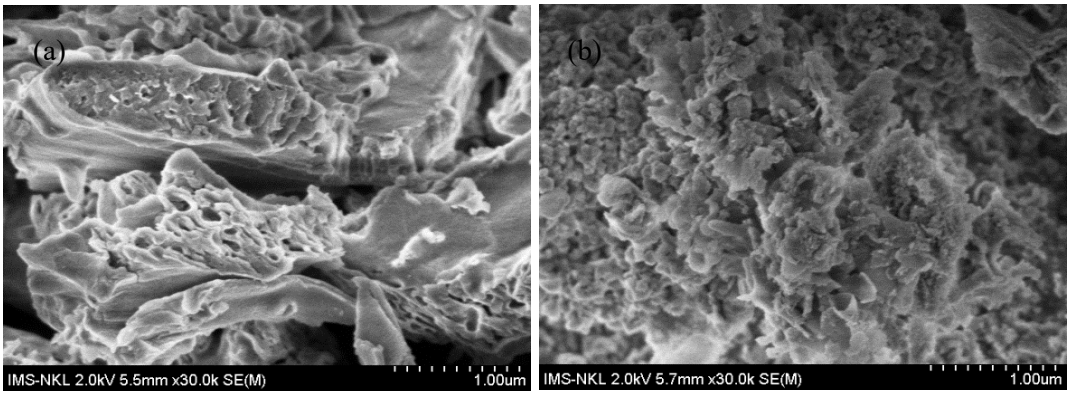

Figure 5. SEM images of g-C_3N_4: (a) bulk and (b) nanosheet.

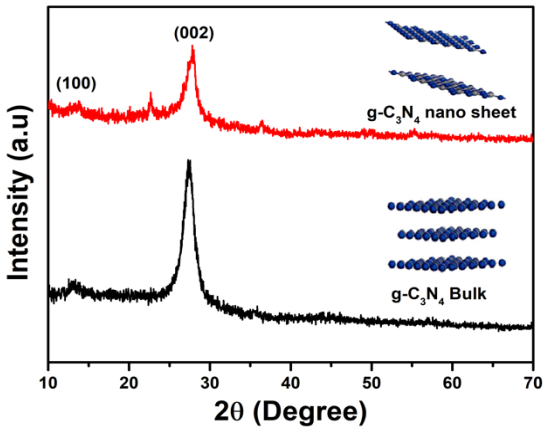

Figure 6. XRD patterns g-C_3N_4 bulk and nanosheet.

Figure 6 shows the XRD patterns of the g-C_3N_4 nanosheet and bulk samples. The results showed that the nanosheet samples exhibited weaker diffraction peak intensity than bulk samples. All samples synthesized from these two precursors showed the appearance of two diffraction peaks, in which a strong diffraction peak at the angle $2\theta = 27.4°$ corresponds to the diffraction surfaces (002), characterizing the superposition of aromatic conjugate systems; Another weaker diffraction peak at $2\theta = 12.78°$ corresponds to the diffraction surface (100), which characterizes the cyclic arrangement of tri-s-triazine or heptazine structural units. In addition, the nanosheet sample has an additional peak at 23° that can be explained by the presence of O_2 when performing the oxidative 'corrosion' process.

3.3. Optical properties of the material

Figure 7 presents the diffuse reflectance spectrum of the g-C_3N_4 bulk and nanosheet samples. In Figure 7(a), it is easy to see that there is a shift in the absorption amplitude towards the short wavelength. Absorption peaks at about 300 - 400 nm characterize the π - π^* transition in conjugated ring systems, including heterocyclic aromatics. The features near 500 nm are due to the n - π^* transition involving free pairs on the N atoms of the triazine ring.

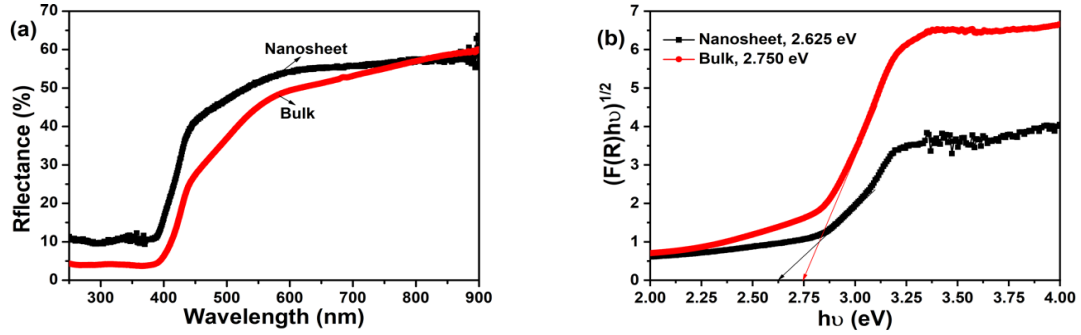

Figure 7. (a) Diffuse reflectance spectra and (b) plot $(F(R)h\nu)^{1/2}$ vs (hν) of g-C_3N_4 bulk and nanosheet.

The optical band gap is extrapolated through the Kubelka-Munk method, where the relationship between incident photon energy hν and the Kubelka-Munk function F(R) follows:

$$(F(R).h\nu = B^*(h\nu - Eg)^n \quad (1)$$

where F(R) is a Kubelka-Munk function determined from the diffuse reflectance R through the formula $F(R) = (1-R)^2/2R$; hν is incident photon energy; and n = 1/2 for direct allowed transitions.

The optical band gap corresponds to 2.750 eV for the g-C_3N_4 bulk and 2.625 eV for the C_3N_4 nanosheets. The narrowing of the optical band gap could be due to various reasons such as the presence of oxygen vacancies and the surface interaction between g-C_3N_4 nanosheet and H_2S or CS_2.

The emission peak of g-C_3N_4 bulk is around 465 nm, whereas the position of the emission peak shows a shift to about 444 nm for g-C_3N_4 nanosheets, consistent with the conditions observed in the UV-vis spectroscopy. The luminescence (PL) spectra of the samples were examined at an excitation wavelength of 340 nm and are presented in Figure 8. The g-C_3N_4 bulk shows very strong emission peaks centered at 437 nm, turning to 454 nm in the nanosheet. This is consistent with the shift of the absorption band edge after calcination and may be due to the high degree of condensation and filling between the layers in the structure. The PL intensity of the g-C_3N_4 nanosheet is lower than the g-C_3N_4 bulk due to the inhibition of the recombination rate of photo-excited electron-hole pairs, which in turn is ascribed to the thin structure of the few-layer g-C_3N_4. This inhibition in the recombination of charge carriers is helpful for the enhancement of photocatalyst performance [22, 23].

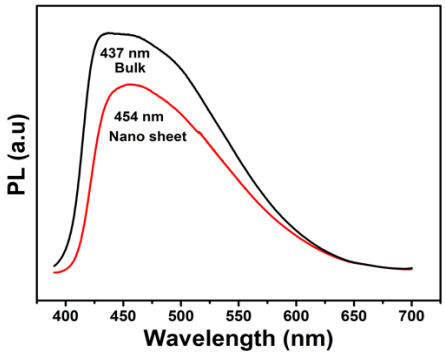

Figure 8. PL spectra of g-C_3N_4 bulk and nanosheet.

Lorentz fitting of the PL peaks helps us obtain a clear understanding of the nature and origin of excitons in the g-C_3N_4 bulk and nanosheet. The R^2 value of fit Lorentz results is greater than 0.97, which is very reliable. Three major emission centers have been demonstrated in the fitting and decomposition of the emission spectrum of the g-C_3N_4 samples. Figure 9(a) shows the line shape analysis of the g-C_3N_4 bulk, which includes the emission center P1 (430 nm, 2.89 eV), P2 (460 nm, 2.70 eV), and P3 (519 nm, 2.39 eV). In Figure 9(b), the emission center P1 (439 nm, 2.83 eV), P2 (470 nm, 2.64 eV), and P3 (511 nm, 2.43 eV) for g-C_3N_4 nanosheet is also presented. According to the previous PL study of g-C_3N_4, the optical bandgap states of g-C_3N_4 consist of a sp^3 C-N σ band, sp^2 C-N π band and the lone pair (LP) state of the bridge nitride atom, and the P1, P2 and P3 origin from the 3 different pathways of transitions: π*-π, σ*-LP and π*-LP, respectively [24]. The emission center of the g-C_3N_4 nanosheet has a shorter shift. This shift can be explained by the extension of the g-C_3N_4 network. When more heptazine is connected by the amino group, the π states will hybridize into a broad state, causing the bandgap narrowing of the sp^2 C–N clusters.

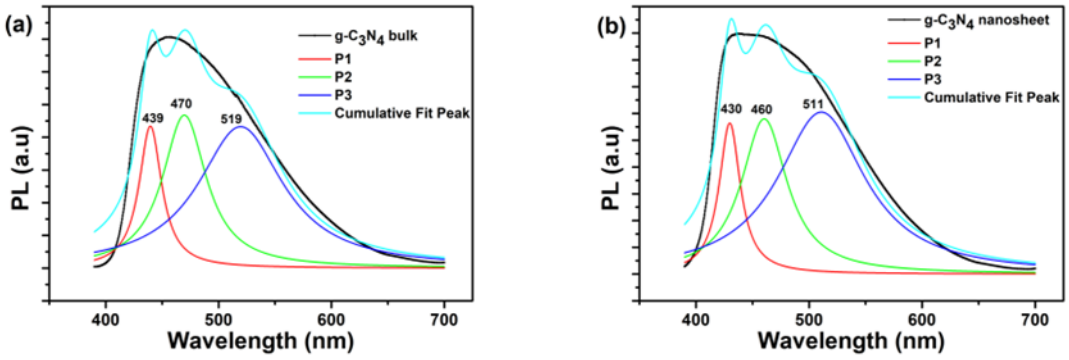

Figure 9. Lorentz fitting of PL emission spectra of the g-C_3N_4 bulk (a) and nanosheet (b) which indicate 3 major PL peaks (P1, P2 and P3).

4. CONCLUSIONS

Polymeric g-C_3N_4 bulk was successfully synthesized with a facile and environmentally benign approach by directly treating low-cost thiourea in air at 550 °C/2 h with a rate of 5 °C/min. Thiourea is a better precursor for the synthesis of g-C_3N_4 bulk than a toxic precursor such as dicyandiamide. The g-C_3N_4 bulk has an optical band gap of around 2.750 eV, while the g-C_3N_4 nanosheet has a narrowing optical bandgap of about 2.625 eV, suitable for visible light utilization. The g-C_3N_4 bulk shows very strong emission peaks centered at 437 nm, turning to 437 nm in the nanosheet. The PL intensity of the g-C_3N_4 nanosheet is lower than the g-C_3N_4 bulk due to the inhibition of the recombination rate of photo-excited electron-hole pairs. This work demonstrates a highly valuable facile method to synthesize high-performance g-C_3N_4 polymeric photocatalysts from easily available thiourea for large-scale environmental and energy applications.

Acknowledgements. We would like to acknowledge the research funding from the Ministry of Education and Training (Grant number: B2023-BKA-04).

Credit authorship contribution statement. Luu Thi Lan Anh: Conceptualization, Supervision, Funding acquisition, Resources. Nguyen Quang Truong: Data curation, Methodology, Investigation, Writing-

Original Draft. Nguyen Thi Tuyet Mai: Methodology, Investigation, Formal analysis. Nguyen Cong Tu: Formal analysis, Data curation, Methodology. Le Manh Cuong: Supervision, Writing - Review & Editing.

Declaration of competing interest. The authors declare that they have no known competing financial interests or personal relationships that could have appeared to influence the work reported in this paper.

REFERENCES

1. Sohail M., Anwar U., Taha T. A., Qazi H. I. A., Al-Sehemi A. G., Ullah S., Algarni H., Ahmed I. M., Amin M. A., Palamanit A., Iqbal W., Alharthi S., Nawawi W. I., Ajmal Z., Ali H., Hayat A. - Nanostructured materials based on g-C_3N_4 for enhanced photocatalytic activity and potentials application: A review. Arab. J. Chem., **15**(9) (2022) 104070. https://doi.org/10.1016/j.arabjc.2022.104070.
2. Alaghmandfard A., Ghandi K. - A Comprehensive Review of Graphitic Carbon Nitride (g-C_3N_4)-Metal Oxide-Based Nanocomposites: Potential for Photocatalysis and Sensing. Nanomaterials (Basel), **12**(2) (2022) 294. https://doi.org/10.3390/nano12020294.
3. Inagaki M., Tsumura T., Kinumoto T., Toyoda M. - Graphitic carbon nitrides (g-C_3N_4) with comparative discussion to carbon materials. Carbon, **141** (2019) 580-607. https://doi.org/10.1016/j.carbon.2018.09.082.
4. Raaja Rajeshwari M., Kokilavani S., Sudheer Khan S. - Recent developments in architecturing the g-C_3N_4 based nanostructured photocatalysts: Synthesis, modifications and applications in water treatment. Chemosphere, **291**(Pt 1) (2022) 132735. https://doi.org/10.1016/j.chemosphere.2021.132735.
5. Abu-Sari S. M., Daud W., Patah M. F. A., Ang B. C. - A review on synthesis, modification method, and challenges of light-driven H_2 evolution using g-C_3N_4-based photocatalyst. Adv. Colloid Interface Sci., **307** (2022) 102722. https://doi.org/10.1016/j.cis.2022.102722.
6. Wang J., Wang S. - A critical review on graphitic carbon nitride (g-C_3N_4)-based materials: Preparation, modification and environmental application. Coord. Chem. Rev., **453** (2022) 214338. https://doi.org/10.1016/j.ccr.2021.214338.
7. Balakrishnan A., Chinthala M. - Comprehensive review on advanced reusability of g-C_3N_4 based photocatalysts for the removal of organic pollutants. Chemosphere, **297** (2022) 134190. https://doi.org/10.1016/j.chemosphere.2022.134190.
8. Kashyap T., Biswas S., Ahmed S., Kalita D., Nath P., Choudhury B. - Plasmon activation versus plasmon quenching on the overall photocatalytic performance of Ag/Au bimetal decorated g-C_3N_4 nanosheets under selective photoexcitation: A mechanistic understanding with experiment and theory. Appl. Catal. B: Environ., **298** (2021) 120614. https://doi.org/10.1016/j.apcatb.2021.120614.
9. Babu B., Shim J., Kadam A. N., Yoo K. - Modification of porous g-C_3N_4 nanosheets for enhanced photocatalytic activity: In-situ synthesis and optimization of NH_4Cl quantity. Catal. Commun., **124** (2019) 123-127. https://doi.org/10.1016/j.catcom.2019.01.009.
10. Dai Y., Wang Y., Zuo G., Kong J., Guo Y., Sun C., Xian Q. - Photocatalytic degradation mechanism of phenanthrene over visible light driven plasmonic Ag/Ag_3PO_4/g-C_3N_4 heterojunction nanocomposite. Chemosphere, **293** (2022) 133575. https://doi.org/10.1016/j.chemosphere.2022.133575.
11. Shi H., Li Y., Wang X., Yu H., Yu J. - Selective modification of ultra-thin g-C_3N_4 nanosheets on the (110) facet of Au/$BiVO_4$ for boosting photocatalytic H_2O_2 production. Appl. Catal. B: Environ., **297** (2021) 120414. https://doi.org/10.1016/j.apcatb.2021.120414.
12. Heydari M., Azizi N., Mirjafari Z., Hashemi M. M. - Aluminum anchored on g-C_3N_4 as robust catalysts for Mannich reaction at ambient temperature. J. Mol. Struct., **1259** (2022) 132731. https://doi.org/10.1016/j.molstruc.2022.132731.

13. Arif M., Li Q., Yao J., Huang T., Hua Y., Liu T., Liu X. - Enhance photocatalysis performance and mechanism of CdS and Ag synergistic co-catalyst supported on mesoporous g-C_3N_4 nanosheets under visible-light irradiation. J. Environ. Chem. Eng., **5**(6) (2017) 5358-5368. https://doi.org/10.1016/j.jece.2017.10.024.
14. Rao S., Li Y., Liu H., Gao S., Zhao J., Rahman N., Li J., Zhou Y., Wang D., Zhang L., Liu Q., Yang J. - Polyethyleneimine induced highly dispersed Ag nanoparticles over g-C_3N_4 nanosheets for efficient photocatalytic and antibacterial performance. Ceram. Int., **47**(6) (2021) 8528-8537. https://doi.org/10.1016/j.ceramint.2020.11.220.
15. Zhang X., Hu K., Zhang X., Ali W., Li Z., Qu Y., Wang H., Zhang Q., Jing L. - Surface co-modification with highly-dispersed Mn & Cu oxides of g-C_3N_4 nanosheets for efficiently photocatalytic reduction of CO_2 to CO and CH_4. Appl. Surf. Sci., **492** (2019) 125-134. https://doi.org/10.1016/j.apsusc.2019.06.189.
16. Yan Y., Zhou X., Yu P., Li Z., Zheng T. - Characteristics, mechanisms and bacteria behavior of photocatalysis with a solid Z-scheme Ag/AgBr/g-C_3N_4 nanosheet in water disinfection. Appl. Catal. A: Gen., **590** (2020) 117282. https://doi.org/10.1016/j.apcata.2019.117282.
17. Zhang X., Jiang S. P., Yang P. - Bright and tunable photoluminescence from the assembly of red g-C_3N_4 nanosheets. J. Lumin., **235** (2021) 118055. https://doi.org/10.1016/j.jlumin.2021.118055.
18. Tong J., Zhang L., Li F., Wang K., Han L., Cao S. - Rapid and high-yield production of g-C_3N_4 nanosheets via chemical exfoliation for photocatalytic H_2 evolution. RSC Adv., **5**(107) (2015) 88149-88153. https://doi.org/10.1039/c5ra16988g.
19. Chang X., Xu S., Wang D., Zhang Z., Guo Y., Kang S. - Flash dual-engineering of surface carboxyl defects and single Cu atoms of g-C_3N_4 via unique CO_2 plasma immersion approach for boosted photocatalytic activity. Mater. Today Adv., **15** (2022) 100274. https://doi.org/10.1016/j.mtadv.2022.100274.
20. Yang L., Huang J., Shi L., Cao L., Yu Q., Jie Y., Fei J., Ouyang H., Ye J. - A surface modification resultant thermally oxidized porous g-C_3N_4 with enhanced photocatalytic hydrogen production. Appl. Catal. B: Environ., **204** (2017) 335-345. https://doi.org/10.1016/j.apcatb.2016.11.047.
21. Kumar A., Singh S., Khanuja M. - A comparative photocatalytic study of pure and acid-etched template free graphitic C_3N_4 on different dyes: An investigation on the influence of surface modifications. Mater. Chem. Phys., **243** (2020) 122402. https://doi.org/10.1016/j.matchemphys.2019.122402.
22. Zhang J., Zhang M., Yang C., Wang X. - Nanospherical carbon nitride frameworks with sharp edges accelerating charge collection and separation at a soft photocatalytic interface. Adv. Mater., **26**(24) (2014) 4121-4126. https://doi.org/10.1002/adma.201400573.
23. Liu D., Tong N., Zhang Z., Yang Z., Wang Y., Li F., Lin H., Long J., Wang X. - Post-synthetic regulation of the structure, morphology and photoactivity of graphitic carbon nitride by heat-vacuum treatment. Mater. Des., **114** (2017) 208-213. https://doi.org/10.1016/j.matdes.2016.11.087.
24. Sharma A., Varshney M., Chae K. H., Won S. O. - Mechanistic investigations on emission characteristics from g-C_3N_4, g-C_3N_4@Pt and g-C_3N_4@Ag nanostructures using X-ray absorption spectroscopy. Curr. Appl. Phys., **18**(11) (2018) 1458-1464. https://doi.org/10.1016/j.cap.2018.08.019.